QIRT'2022
10.21611/qirt.2022.2004
16th Quantitative InfraRed Thermography Conference

A simulation study into the effect of the defect type and excitation non-uniformity on the defect detectability with flash thermography

by G. Poelman*, S. Hedayatrasa* and M. Kersemans*

* Mechanics of Materials and Structures (UGent-MMS), Department of Materials, Textiles and Chemical Engineering (MaTCh), Ghent University, Technologiepark-Zwijnaarde 46, 9052 Zwijnaarde, Belgium, *Gaetan.Poelman@UGent.be*

Abstract

Flash thermography is a valuable testing methodology to perform a rapid, full-field, non-destructive inspection. Many researchers have investigated the physical detection limits of flash thermography, however, those studies differ from one another in many ways (e.g. different defect properties). As such, it is difficult to combine their results into a general overview of the true defect detection limits in flash thermography. Therefore, the present authors have performed a parametric study into the defect detection limits of flash thermography using 3D finite element modelling. In this contribution, the influence of the defect type and excitation non-uniformity on the detection limits are discussed.

1. Introduction

Flash thermography (FT) is a valuable non-destructive testing (NDT) method to rapidly inspect a thermally conductive material for hidden defects. [1-3] While the raw flash thermographic recordings are useful to have a fast indication of the inspected part's structural health, the application of advanced post-processing algorithms is indispensable to ensure an accurate and reliable evaluation. [4-12] Over the course of the past few decades, many researchers have explored the influence of various parameters on the detectability of defects through (post-processed) FT. [13-24] While all these studies have provided profound insights into the phenomena affecting the defect detectability, they cannot be easily combined in order to generate a clear overview of the actual physical defect detection limits of FT due to the significant differences in their material and testing conditions:

- methodology: (1D) analytical, finite element modelling or experimental,
- analysis type: unprocessed thermal data, PPT, TSR, …,
- excitation settings: heating power and non-uniform heating profile,
- material parameters: thermal properties, stacking sequence, …,
- …

In order to fill this gap in the current literature, the present authors have performed a large-scale 3D finite element (FE) study where the defect detectability of FT is studied in detail. This contribution expands on two important factors: (i) the defect type, and (ii) the excitation non-uniformity. The study does not limit itself to the raw thermographic results, but further also considers several often-applied post-processing algorithms. The remainder of this manuscript is constructed as follows: section 2 briefly explains the methodology of the presented study, after which the results are presented in section 3. Finally, concluding remarks are provided in section 4.

2. Methodology

A schematic overview of the FE simulation model in this study is presented in *Figure 1*. Two flash lamps provide a square test coupon with an optical excitation of 5 ms, and are located at a fixed location with respect to the center of the coupon. The average heat flux deposited onto the test coupon is 0.56 $\mathrm{W\,mm^{-2}}$. Note that these lamps are identical and symmetrically placed in order to reduce the calculation efforts by a factor of 2.

The FE model considers a 24-ply composite material with a total thickness of 5.5 mm (ply thickness ~0.23 mm). In this contribution, the results are presented for a carbon fiber reinforced polymer (CFRP) with a cross-ply layup of $[(0/90)_6]_s$ and an emissivity of 0.9. The defect is located at the center of the simulated test coupon, with a sufficiently large sound area surrounding it for reliable contrast-to-noise ratio (CNR) calculations. In total, 10 defect sizes are considered, ranging from 1 mm up to 30 mm. The defects are positioned at all inter-ply locations, covering a defect depth range from 0.23 mm to 5.27 mm. This study thus covers defect aspect ratios (= ratio of in-plane defect size to defect depth) from 0.19 to 130.4. Heat exchange with the surroundings are considered through radiative and convective heat losses at the top and bottom surfaces of the test coupon. The considered ambient temperature is 25 °C. For each simulation, the cooling down regime is calculated for 120 s at a sampling frequency of 20 Hz, after which white Gaussian noise with a noise equivalent differential temperature (NEDT) of 15 mK is added to mimic measurement noise of a cooled infrared camera. All FE simulations are performed using the commercial FE software Abaqus CAE with an implicit solver.

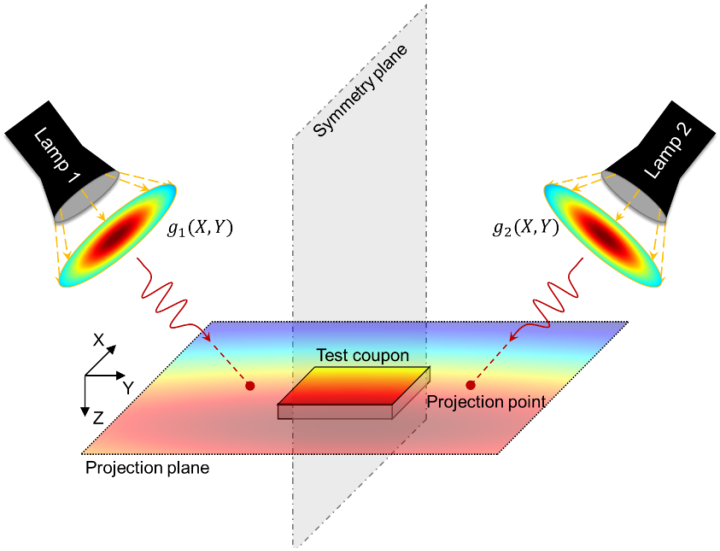

Figure 1: Schematic illustration of the used finite element model.

For this contribution, the raw thermographic data is additionally post-processed with two often-used data analysis techniques for FT, namely Pulsed Phase Thermography (PPT) [10, 25] and Thermographic Signal Reconstruction (TSR) [6, 26]. Next, the CNR is calculated for each simulated scenario, which is then used as metric to quantify a defect's detectability. These CNR values are divided into four categories to provide further qualitative information about the defect detectability:

- $CNR > 4$: Good detectability,
- $2 < CNR \leq 4$: Intermediate detectability,
- $1 < CNR \leq 2$: Poor detectability,
- $CNR \leq 1$: Undetectable.

It is important to remark that the calculated CNR values have shown an excellent match with experimental observations, and are thus representative of real experimental scenarios. For conciseness, the experimental validation is not presented here.

3. Results

3.1. Defect type

One of the main parameters that is known to affect a defect's detectability is of course the defect type itself. The effect of the defect type is in this section investigated for the 24-ply cross-ply CFRP component, with a uniform excitation and a 15 mK noise level. In total, six different defect types are considered. The thermal reflection coefficient $R_{CFRP-def}$ and the defect's thermal resistance W_{th} of each defect type are listed in Table 1, and are calculated as follows:

$$R_{CFRP-def} = \frac{e_{CFRP} - e_{def}}{e_{CFRP} + e_{def}} \quad (1)$$

$$W_{th} = \frac{t_{def}}{k_{def}} \quad (2)$$

where e_{CFRP} and e_{def} are the thermal effusivity of CFRP and the defect, respectively. t_{def} and k_{def} are respectively the defect's thickness and thermal conductivity.

Table 1: Thermal reflection coefficient and thermal resistance of the considered defect types.

Defect type	**Thermal reflection coefficient** $R_{CFRP-def}$ [-]	**Thermal resistance** W_{th} [m^2 K W^{-1}]
FBH	1	$\rightarrow \infty$
Disconnected nodes	1	∞
Air insert of 100 µm	1	4.0 e^{-3}
Air insert of 13 µm	1	5.2 e^{-4}
Polyurethane insert of 13 µm	0.95	4.3 e^{-4}
PTFE insert of 13 µm	0.11	5.2 e^{-5}

The obtained CNR values (in $\log_{10}$-scale) of the raw thermographic sequence for the different defect types are presented in *Figure 2*. As could be expected, the FBH's (*Figure 2*(a)) and disconnected nodes (*Figure 2*(b)) provide the best defect detectability since they have the highest thermal reflection coefficient and thermal resistance. Only for smaller defect sizes (i.e. the bottom rows), the disconnected nodes provide a reduced defect detectability, which is a results of the in-plane lateral heat diffusion (more prominent for smaller defects), which allows the heat to also flow away below the defect and thus leads to a more efficient heat dissipation. An air insert of 100 µm (*Figure 2*(c)) provides a reduced defect detectability as it also allows heat transfer directly through the defect itself (i.e. no infinite thermal resistance). Further reducing the defect thickness to 13 µm (*Figure 2*(d)) results in a lower thermal resistance, which makes the heat transport through the defect more effective, resulting in a worsened defect detectability. As highlighted in [17], polyurethane has highly similar thermal properties as air, which is indeed observed by comparing its defect detectability with the one of an air insert of identical thickness (*Figure 2*(d,e)). Lastly, the defect detectability levels of a polytetrafluorethylene (PTFE) insert are very low (*Figure 2*(f)). While this defect type is often the preferred one in experimental studies in the field of infrared thermography, the results clearly demonstrate that it is not representative of an air layer inside the composite material.

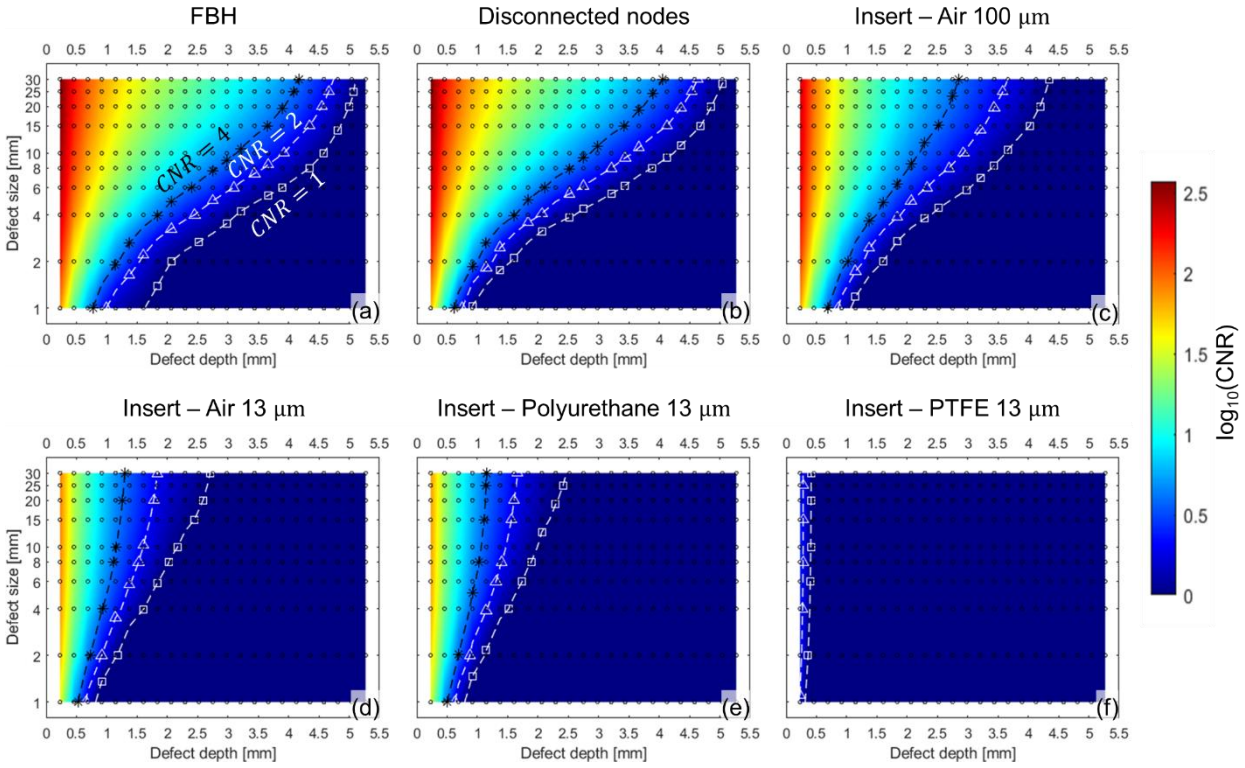

Figure 2: The effect of defect type on the defect detectability of the raw thermographic sequence (CFRP, cross-ply, uniform heating, 15 mK noise).

All other consider post-processing algorithms provide identical conclusions about the relative defect detectability of the different defect types, and are therefore omitted for conciseness.

Since the air insert of 13 µm thickness is the most representative of a delamination defect in composites [27], this defect type is further used to study the effect of the excitation non-uniformity.

3.2. Excitation non-uniformity

Next, the influence of the excitation non-uniformity on the defect detectability of an air insert of 13 μm thickness is studied in this section. For both the uniform and non-uniform excitation, the same average heat flux of 0.56 $W\,mm^{-2}$ is applied to the test coupon. The shape of the non-uniform excitation was first determined experimentally by matching the deposited heat profile to a bivariate normal distribution. The studied case is a CFRP cross-ply sample of 5.5 mm thick, with an air insert of 13 μm thickness, and 15 mK noise.

The influence of the excitation non-uniformity on the calculated CNR values (in $\log_{10}$-scale) are visualized in *Figure 3*. The different rows present the results for the raw thermographic sequence, PPT, and the TSR coefficients. The left column are the results for the uniform excitation and the middle column for the non-uniform excitation. The right column also presents results for non-uniform excitation, but where a temporal standardization is applied as pre-processing step in order to reduce the effects of background non-uniformity. [5]

It is immediately clear that the excitation non-uniformity has detrimental effects on the defect detectability for both the raw temperature and the TSR coefficients. This is a result of the definition of CNR, where the standard deviation in the sound area has an inversely proportional effect on the CNR. Since the non-uniformity in the sound area is high for the large defects (since the sound area scales with the defect size), this results in very low CNR values.

For the raw temperature (*Figure 3*, top row), applying a temporal standardization is an important pre-processing step to obtain good defect detectability (*Figure 3*(c)). Moreover, the standardization increases the defect contrast and reduces the noise level with respect to the uniform excitation, resulting in higher CNR values and improved defect detection limits (i.e. $\mathrm{CNR} = 1$).

The results for PPT (*Figure 3*, middle row) highlight lower CNR levels than the raw temperature, but with significantly improved defect detection limits. Due to the steps involved in the calculation of the phase values for PPT, there is only a slight reduction in defect detectability between the uniform and non-uniform excitation cases (*Figure 3*(d,e)). Additionally, applying a standardization as pre-processing does not affect the results of PPT (see *Figure 3*(f)).

Lastly, the TSR coefficients (*Figure 3*(g)) provide the highest CNR values and best detection limits of the presented post-processing techniques. Also here, applying a temporal standardization is required to effectively counteract the effects of the non-uniform excitation (*Figure 3*(h,i)). Comparable CNR values and detection limits are obtained between the uniform excitation and the standardized non-uniform excitation. Additionally, the results for the TSR derivatives provide comparable insights and are therefore omitted.

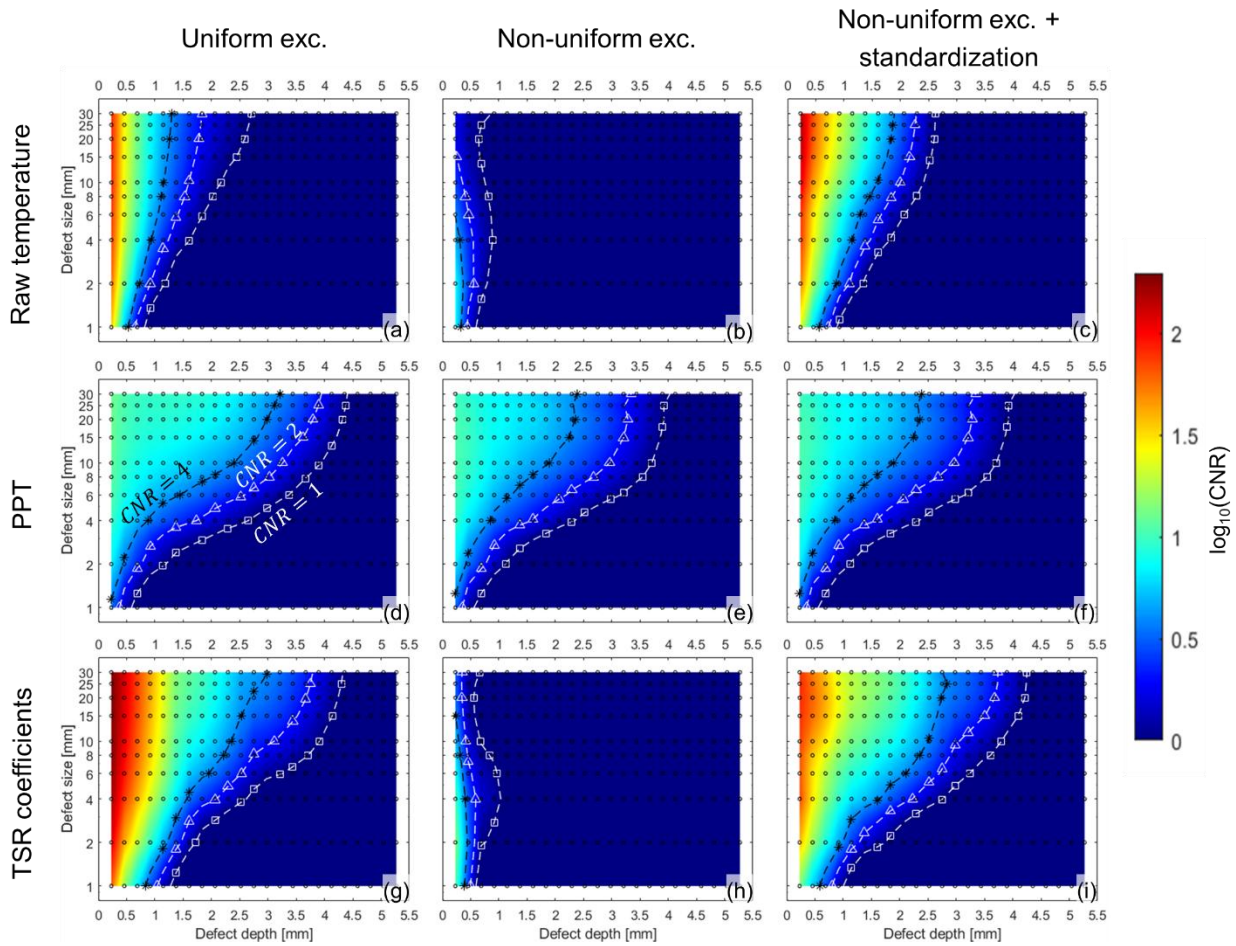

Figure 3: The effect of excitation non-uniformity on the defect detectability of a 13 μm air insert (CFRP, cross-ply, 13 μm air insert, 15 mK noise): (left column) uniform excitation, (middle column) non-uniform excitation, and (right column) non-uniform excitation with temporal standardization. Different processing algorithms are shown: (top row) raw thermographic sequence, (middle row) PPT, and (bottom row) TSR coefficients.

4. Conclusions

In this contribution, a 3D finite element study is presented to investigate the defect detection limits of flash thermography for different defect types and excitation non-uniformities. A wide range of defect sizes and defect depths are considered, covering aspect ratios from 0.19 to 130.4. Results are discussed for the (standardized) raw thermographic sequence, as well as for PPT and TSR processed thermographic data.

The defect type was observed to have a primordial effect on its detectability. FBH's and disconnected nodes are the easiest to detect, whereas PTFE inserts are almost undetectable. The defect detectability dropped with a reducing thermal reflection coefficient and thermal resistance. The presented results confirm the finding of a recent study [17], namely that polyurethane inserts are a practical way to mimick realistic delaminations in a composite.

In actual applications, the heating profile of optical lamps tends to be spatially non-uniform. The presented results indicate a reduced defect detectability in case of a non-uniform heating profile. The application of a temporal standardization on the thermal data can counteract the negative effects of the excitation non-uniformity to some extent.

ACKNOWLEDGEMENTS

The authors acknowledge Fonds voor Wetenschappelijk Onderzoek-Vlaanderen (FWO-Vlaanderen) through grant 1S11522N and Bijzonder Onderzoeksfonds (BOF) through grant (BOF21/PDO/041).

REFERENCES

1. Nsengiyumva, W., et al., *Advances, limitations and prospects of nondestructive testing and evaluation of thick composites and sandwich structures: A state-of-the-art review.* Composite Structures, 2020: p. 112951.
2. Towsyfyan, H., et al., *Successes and challenges in non-destructive testing of aircraft composite structures.* Chinese Journal of Aeronautics, 2019.
3. Moskovchenko, A., et al., *Analyzing probability of detection as a function of defect size and depth in pulsed IR thermography.* NDT & E International, 2022.
4. Fleuret, J.R., et al., *Independent Component Analysis Applied on Pulsed Thermographic Data for Carbon Fiber Reinforced Plastic Inspection: A Comparative Study.* Applied Sciences, 2021. **11**(10).
5. Poelman, G., et al., *An Experimental Study on the Defect Detectability of Time- and Frequency-Domain Analyses for Flash Thermography.* Applied Sciences, 2020. **10**(22): p. 8051.
6. Balageas, D.L., et al., *The Thermographic Signal Reconstruction Method: A Powerful Tool for the Enhancement of Transient Thermographic Images.* Biocybern Biomed Eng, 2015. **35**(1): p. 1-9.
7. Krapez, J.-C., *Thermal Contrasts in Pulsed Infrared Thermography*, in *Chapter 13, Nondestructive Testing Handbook. Vol 3: Infrared and Thermal Testing*, X.P.V. Maldague and P.O. Moore, Editors. 2001, The American Society for Non Destructive Testing (ASNT). p. 411-439.
8. Rajic, N., *Principal component thermography for flaw contrast enhancement and flaw depth characterisation in composite structures.* Composite Structures, 2002. **58**(4): p. 521-528.
9. Poelman, G., et al., *Adaptive spectral band integration in flash thermography: Enhanced defect detectability and quantification in composites.* Composites Part B: Engineering, 2020. **202**: p. 108305.
10. Maldague, X. and S. Marinetti, *Pulse Phase Infrared Thermography.* Journal of Applied Physics, 1996. **79**(5): p. 2694-2698.
11. Oswald-Tranta, B., *Time and frequency behaviour in TSR and PPT evaluation for flash thermography.* Quantitative InfraRed Thermography Journal, 2017. **14**(2): p. 164-184.
12. Ibarra-Castanedo, C., et al., *On signal transforms applied to pulsed thermography.* Recent Res. Devel. Applied Phys., 2006. **9**.
13. Oswald-Tranta, B., *Comparative study of thermal contrast and contrast in thermal signal derivatives in pulse thermography.* NDT & E International, 2017. **91**: p. 36-46.
14. Oswald-Tranta, B., R. Schmidth, and T. Grandl. *Comparison of samples with flat bottom holes and with hidden occlusions using flash thermography*. in *13th Quantitative InfraRed Thermography Conference (QIRT 2016)*. 2016. Quebec, Canada.
15. Wallace, N.J., N.B. Crane, and M.R. Jones, *Defect measurement limits using flash thermography with application to additive manufacturing.* NDT & E International, 2022.
16. Cotič, P., et al., *Determination of the applicability and limits of void and delamination detection in concrete structures using infrared thermography.* NDT & E International, 2015. **74**: p. 87-93.
17. Moradi, M. and M.S. Safizadeh, *Experimental and numerical study of the effect of using polyurethane instead of Teflon strip to simulate debonding defect in composite patch repairs aluminum plate under thermography inspection.* Composites Part B: Engineering, 2019. **175**.
18. Popow, V. and M. Gurka, *Full factorial analysis of the accuracy of automated quantification of hidden defects in an anisotropic carbon fibre reinforced composite shell using pulse phase thermography.* NDT & E International, 2020. **116**: p. 102359.
19. Meola, C., G.M. Carlomagno, and L. Giorleo, *Geometrical Limitations to Detection of Defects in Composites by Means of Infrared Thermography.* Journal of Nondestructive Evaluation, 2004. **23**(4): p. 125-132.
20. Ishikawa, M. and M. Koyama, *Influence of Composite Ply Layup on Active Thermographic Non-destructive Inspection of Carbon Fiber-Reinforced Plastic Laminates.* Journal of Nondestructive Evaluation, 2018. **37**(2).
21. Krishnapillai, M., et al., *NDTE using pulse thermography: Numerical modeling of composite subsurface defects.* Composite Structures, 2006. **75**(1-4): p. 241-249.
22. Montanini, R. and F. Freni, *Non-destructive evaluation of thick glass fiber-reinforced composites by means of optically excited lock-in thermography.* Composites Part A: Applied Science and Manufacturing, 2012. **43**(11): p. 2075-2082.
23. Almond, D.P. and S.G. Pickering, *An analytical study of the pulsed thermography defect detection limit.* Journal of Applied Physics, 2012. **111**(9).
24. Vavilov, V.P., *3D modeling of pulsed thermal NDT: Back to basic features and subtle phenomena.* NDT & E International, 2022. **130**.
25. Ibarra-Castanedo, C. and X. Maldague, *Pulsed phase thermography reviewed.* Quantitative InfraRed Thermography Journal, 2004. **1**(1): p. 47-70.
26. Shepard, S.M., *Temporal noise reduction, compression and analysis of thermographic data sequences*. 2003, Thermal Wave Imaging, Inc.: US.
27. D5528-01, A., *Standard Test Method for Mode I Interlaminar Fracture Toughness of Unidirectional Fiber-Reinforced Polymer Matrix Composites*. ASTM International: West Conshohocken, PA, 2001.